THE ASTROPHYSICAL JOURNAL, 440:853–864, 1995 February 20

A RADIAL VELOCITY STUDY OF THE DWARF NOVA AR ANDROMEDAE: COMPARISON OF THE QUIESCENT AND OUTBURST STATES

A. W. SHAFTER[1] AND J. M. VEAL[2]
Department of Astronomy and Mount Laguna Observatory, San Diego State University, San Diego, CA 92182;
shafter@proteus.sdsu.edu; veal@sirius.astro.uiuc.edu

AND

E. L. ROBINSON
Department of Astronomy, University of Texas, Austin, TX 78712; elr@aries.as.utexas.edu
Received 1994 June 9; accepted 1994 September 2

ABSTRACT

Radial velocity studies of the dwarf nova AR And during quiescence and eruption are presented and compared. These data strongly suggest the orbital period is 0.1640 ± 0.0005 days, although 1 cycle day^{-1} aliases of this period cannot be ruled out unequivocally. Despite being formed in dissimilar disk environments, the quiescent emission and outburst absorption lines yield similar radial velocity amplitudes. The quiescent emission-line amplitude obtained from measurements of Hα is $K_{em} = 83 \pm 7$ km s^{-1}. The amplitude during outburst, as determined from analysis of the Hβ and Hγ absorption lines is slightly lower, but consistent with the quiescent value. Observations obtained on 1991 December 10, $\sim$1 week after outburst maximum, yielded $K_{abs} = 74 \pm 10$ km s^{-1} for both Hβ and Hγ. The following night the lines were weaker, the data noiser, and the spectra fewer, resulting in less reliable velocity amplitudes. Nevertheless, the average amplitude of 73 ± 16 km s^{-1} is consistent with the amplitudes determined on the previous night.

The similarity between the emission- and absorption-line amplitudes in AR And is a robust result. The derived velocity amplitudes are insensitive to the portion of the line profiles used in the velocity measurements, suggesting that the disk radiation is nearly axisymmetric. This result is corroborated by a Doppler tomogram of the quiescent Hα data, which shows that the emission is distributed fairly evenly over the surface of the disk. The results presented here add confidence that velocity variations of spectral features from the accretion disk in AR And may provide a reliable tracer of the orbital motion of the white dwarf in this system.

Subject headings: binaries: spectroscopic — novae, cataclysmic variables — stars: individual (AR Andromedae)

1. INTRODUCTION

Cataclysmic variables are interacting binary stars consisting of a white dwarf star accreting material via an accretion disk from a late-type, near–main-sequence companion. Although all cataclysmic variables are binary stars, the task of determining the masses of these systems is not straightforward and historically has been plagued with difficulties. A principal stumbling block has been the measurement of the radial velocity amplitude of the white dwarf component. This quantity can almost never be measured directly because of the relatively low luminosity of the white dwarf compared with the accretion disk. Consequently, radial velocity studies of cataclysmic variables consist almost exclusively of measurements of the velocity variations of the disk emission, which is *assumed* to reflect the motion of the white dwarf. There is ample reason to suspect, however, that this assumption is usually not justified.

There is compelling evidence that the emission from disks in many cataclysmic variables is highly nonaxisymmetric, not just in the outer regions of the disk near the bright spot as previously thought, but extending well into the disks. The degree and extent of the asymmetry has only recently begun to be fully appreciated. This appreciation has come in large part due to two diagnostic procedures for analyzing time-resolved spectroscopy. The first, and simplest technique involves the "diagnostic diagram" (Shafter 1985). In this procedure, one measures several sets of radial velocities, with each set based on measurements from different positions (velocities) in the emission-line profile. The orbital elements determined from each set of measurements are then plotted as a function of the position in the line profile that was used in measuring the radial velocities. Clearly, systems with axisymmetric disk emission will have emission-line profiles that are not orbital phase dependent. The orbital elements will not depend on whether one bases the velocity measurements on the peak or wings of the emission lines. In systems where the emission is nonaxisymmetric, the situation is more complex. If an excess emission component is confined to the outer regions of the disk (i.e., to near line center), the inferred orbital elements should converge to the true orbital elements as the measurements are made further out into the line wings. This is rarely the situation, however, and the orbital elements typically fail to converge to stable solutions, even in the extreme line wings. Shafter, Hessman, & Zhang (1988), in their study of the eclipsing nova-like variable DW UMa, and other authors in similar studies, have interpreted these diagrams as suggesting that the interstar mass transfer stream penetrates well into the disk causing the disk emission to be nonaxisymmetric even in its inner regions.

A second, newer, and more informative diagnostic technique, Doppler tomography, has been pioneered by Marsh &

[1] Guest observer, McDonald Observatory.
[2] Current address: Astronomy Department, University of Illinois, Urbana, IL 61801.

Horne (1988). In this technique, one reconstructs an image of the accretion disk in velocity coordinates. The resulting images, or "tomograms," reveal directly any asymmetries in the disk's emission-line surface brightness distribution. There are several systems where regions of enhanced emission extend well into the disk, resulting in highly asymmetric disk images (e.g., Kaitchuck 1994). The most pathological cases seemed to include the nova-like variables with periods just above the period gap. Not coincidentally, these are the same systems that show the most distorted radial velocity solutions, where velocity amplitudes seem to be anomalously high, and huge phase offsets are common between spectroscopic conjunction (as defined by the disk emission) and photometric, or true, conjunction. These properties led Thorstensen et al. (1991, 1992) to propose that such systems are not anomalies, but form a relatively common subclass of cataclysmic variables. They proposed that such systems be dubbed the "SW Sex stars."

Despite mounting evidence that the emission-line radial velocity curves are biased in many if not all cataclysmic variables, the nature and extent of the bias is not well understood. It is clear that the nonaxisymmetric disk emission can affect both the amplitude and the phase of the radial velocity curve, but the extent to which either are affected depends on the specific geometry of the emission-line region. Unfortunately, in almost all cases we have no independent determination of the white dwarf's orbital motion, and hence no reliable test of the accuracy with which the emission lines reflect the radial velocity of the white dwarf.

One exception is the DQ Her system, AE Aqr. This system exhibits a coherent 33 s periodicity in its light curve that is caused by the rotation of an accreting magnetized white dwarf (Patterson 1979). Robinson, Shafter, & Balachandran (1991) have recently inferred the semiamplitude of the white dwarf from the measured Doppler shifts of the pulse arrival times. Their photometric determination of the white dwarf's semiamplitude ($K_{\rm pulse} = 122 \pm 4$ km s^{-1}) is slightly lower than the spectroscopically determined value ($K_{\rm em} = 141 \pm 8$ km s^{-1}). In addition, Robinson et al. found what appeared to be a 60° phase offset between the emission-line orbit and the pulse-timing orbit. Since the emission-line orbit was almost exactly 180° out of phase with the absorption-line orbit of Feldt & Chincarini (1980), Robinson et al. concluded that the pulse-timing orbit was distorted and the emission-line orbit was a better tracer of the white dwarf's orbital motion. Recently, however, Welsh, Horne, & Gomer (1993) recomputed the absorption-line ephemeris of Feldt & Chincarini and showed that it had been in error. Their analysis revealed that it is the pulse-timing orbit, and *not* the emission-line orbit that is 180° out of phase with the absorption-line radial velocities. Thus, the emission-line orbit is actually distorted, and it is the pulse-timing orbit after all that is the better tracer of the white dwarf's motion. Unfortunately, since the vast majority of systems do not exhibit coherent pulsations from the white dwarf, the technique used in the AE Aqr study cannot be applied to most cataclysmic variables. There is, however, in the case of dwarf novae, another alternative to relying solely on the disk emission lines to infer the orbital motion of the white dwarf: One can measure the radial velocity variations of the absorption lines during the eruptions of dwarf novae.

When a dwarf nova erupts, the accretion disk becomes bright and optically thick and the emission typically transforms to absorption. In many cases, it is possible to use the absorption lines that are present during the eruptions of dwarf novae in a radial velocity study. Because the absorption lines are produced under markedly different physical conditions than the quiescent-state emission lines, they provide an additional, though not strictly independent, measurement of the white dwarf's semiamplitude. Although there is, as yet, no compelling evidence that the absorption-line velocities will reflect the motion of the white dwarf with any greater reliability than do the emission-line velocities, the additional constraint on the white dwarf's orbital motion will aid in interpreting time-resolved observations of cataclysmic variables.

To date there have been only a few published reports of radial velocity studies of dwarf novae in outburst. In an early study, Hessman (1986) studied SS Cyg and found that the absorption-line semiamplitude derived during outburst agreed well with the quiescent emission-line value. However, a later study of RX And by Kaitchuck, Mansperger, Hantzios (1988) was somewhat less encouraging. Although they found consistency between the quiescent and outburst amplitudes of RX And, the absorption-line profiles appeared to be distorted in a way similar to that seen in the quiescent emission lines. More recently Szkody and collaborators (Feinswog, Szkody, & Garnavich 1988; Szkody, Piché, Feinswog 1990) published radial velocity studies of RX And and three additional systems: IR Gem, AR And, and TW Vir. Despite the paucity of data, the absorption-line amplitudes for these systems are generally consistent within the formal errors (which are rather large due to limited data) with the emission-line amplitudes obtained during quiescence.

Clearly, additional radial velocity studies should be undertaken, and reliable absorption-line orbits determined, before one can properly assess the significance of the pioneering studies mentioned above. Unlike the situation with the pulse-timing measurements of short-period DQ Her systems, we are fortunate in this case to have a wealth of additional dwarf nova systems that are suitable for further study. We are currently in the midst of a program to determine spectroscopic orbits during outburst for a sample of dwarf novae. In this paper we present new and more extensive time-resolved spectroscopic observations of the dwarf nova AR And, both in quiescence and in eruption.

2. OBSERVATIONS

On 1991 December 10, we were alerted by the AAVSO that the dwarf nova AR And was in outburst. We were particularly fortunate that this dwarf nova was in outburst during our observing run because one of us (A. W. S.) had already obtained quiescent radial velocity observations of AR And a few years earlier at the Mount Lemmon Observatory. A visual light curve of AR And spanning the dates of our observations was kindly provided by J. Mattei of the AAVSO (Mattei 1993) and is shown in Figure 1. These data reveal that AR And erupted sometime between 1991 December 3 and 4, ~1 week prior to our initial spectroscopic observations. The details of our spectroscopic observations are described below and are summarized in Table 1.

2.1. *Quiescent Observations*

The quiescent data were obtained as part of a general spectroscopic program to determine the orbital periods of cataclysmic variables. The program was conducted with the University of Minnesota/UCSD Mount Lemmon 1.5 m reflector, which was equipped with an image dissector scanner (IDS) (see Robinson & Wampler 1972). The IDS produces data having

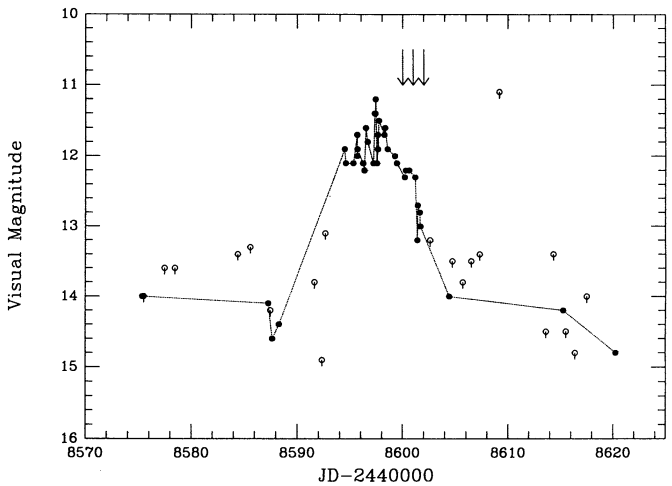

FIG. 1.—AAVSO light curve of AR And during the period covered by our outburst observations. The outburst began sometime between JD 2,448,593 and JD 2,448,594 (1991 December 3 and 4). Filled circles indicate visual magnitude estimates; open circles are upper limits. The arrows indicate the times of our spectroscopic observations, which began ~1 week into the outburst.

2048 spectral channels with a resolution of ~6 channels FWHM. A 1200 line mm^{-1} grating was used, resulting in a reciprocal dispersion of ~0.65 Å $channel^{-1}$ centered at Hα. Consequently, the spectra span ~1300 Å at a spectral resolution of 4 Å. The observations were obtained through two circular apertures ~3.″2 in diameter. AR And was centered in one aperture, while the other simultaneously monitored the sky. The star and sky were alternated between the two apertures, A and B, in the sequence ABBA in order to remove linear trends in sky brightness. The individual integrations have a time resolution of 4 minutes that were later summed into 16 minute sky-subtracted spectra.

The Mount Lemmon IDS is remarkably stable. Repeated neon arc exposures indicate a spectral instability of less than 0.05 channels. The positions of the comparison lines do shift as the telescope tracks, but in a systematic and well-defined fashion. In order to monitor the instrumental shift during our observations, we took neon arc spectra every 32 minutes (i.e., every ABBA sequence has an adjacent arc spectrum). This procedure resulted in an instrumental wavelength stability of ~0.1 channel (3 km s^{-1}).

2.2. *Outburst Observations*

The outburst observations were obtained at McDonald Observatory during the period 1991 December 10–12. These data were obtained using the large Cassegrain spectrograph on the 2.7 m reflector. The spectrograph employed a TI 800 × 800 format CCD detector having a readout noise of ~13e^{-}. By using a 1200 line mm^{-1} grating in first order, we obtained about 900 Å of coverage at a reciprocal dispersion of ~0.9 Å $pixel^{-1}$, centered at Hα. A slit width of ~2″ (set by the seeing) resulted in a spectral resolution of ~2 Å FWHM. All individual integrations were bracketed by brief exposures of an argon arc lamp to define the wavelength calibration and assure velocity stability throughout the sequence of exposures.

3. RADIAL VELOCITY MEASUREMENTS

Radial velocities were measured by convolving the data with a template spectrum, $G(x)$, consisting of two narrow Gaussians (Schneider & Young 1980). The template is positioned so that one Gaussian is positioned in the blue wing and the other in the red wing of the line being measured. The wavelength of the template spectrum is adjusted using a Newton-Raphson iteration procedure until the fluxes through the two bandpasses are equal. The wavelength of the midpoint between the Gaussians is taken as the wavelength of the spectral line. This technique allows the orbital-phase-dependent structure of the line to be probed by making several sets of measurements, each having a different Gaussian separation (e.g., Shafter 1983).

3.1. *The Orbital Period*

We began our analysis by determining the orbital period of AR And. Because of the long interval between the quiescent and outburst observations, the two data sets could not be phased without severe aliasing and were therefore analyzed independently. The first step was to measure velocities for the individual spectra. Unlike the other orbital elements, the value of the orbital period is relatively insensitive to the value of the Gaussian separation. Based on a visual inspection of the data, we chose initial values of $s = 1200$ km s^{-1} and $s = 2200$ km s^{-1} for the quiescent and outburst data, respectively. There is no strongly preferred value for the width of the Gaussian bandpasses. The width is set by considering the spectral resolution of the data and the width of the spectral feature to be measured. Generally, narrow lines suggest narrow bandpasses, while low resolution suggests wide bandpasses. Although the emission lines are narrower than the absorption lines, their resolution is also lower. We have therefore decided to be consistent and use the same Gaussian width in both cases. Specifically, we adopt $\sigma = 300$ km s^{-1} for all measurements.

After measuring the velocities, we searched for periodicities in the data using the Press & Rybicki (1989) algorithm for the Lomb-Scargle periodogram (Lomb 1976; Scargle 1982). The resulting quiescent and outburst periodograms, based on mea-

TABLE 1

SUMMARY OF OBSERVATIONS

HJD (2,440,000+)	Observer	Telescope	Integration Time (minutes)	Number of Spectra	Resolution (Å)
		Quiescent Hα			
6,434	A. W. S.	Mount Lemmon 1.5 m	16	14	4
6,435	A. W. S.	Mount Lemmon 1.5 m	16	13	4
6,436	A. W. S.	Mount Lemmon 1.5 m	16	12	4
		Outburst Hγ and Hβ			
8,600	A. W. S./E. L. R.	McDonald 2.7 m	10	29	2
8,601	A. W. S./E. L. R.	McDonald 2.7 m	10	15	2
8,602	A. W. S./E. L. R.	McDonald 2.7 m	10	10	2

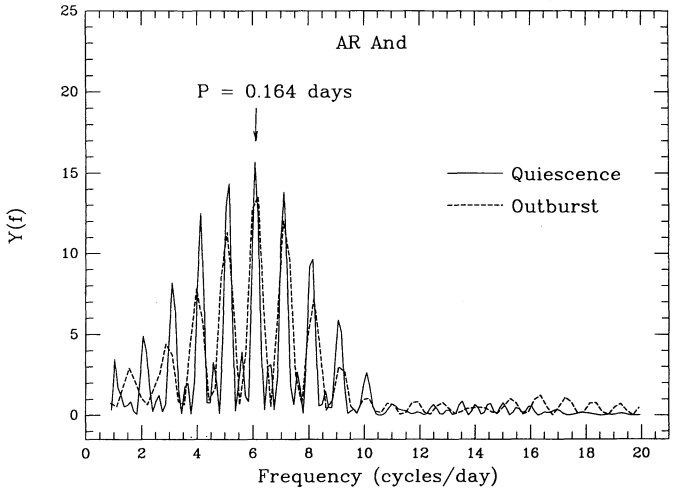

FIG. 2.—Lomb-Scargle periodograms of the quiescent and outburst data. The most probable orbital period is 0.1640 days. The peaks spaced at ± 1, 2, 3 ... cycles per day^{-1} are aliases of the orbital period.

surements of Hα emission and Hβ absorption, respectively, are shown in Figure 2. The quiescent data favor an orbital period of 0.1640 ± 0.005 days. The other peaks in the periodogram correspond to aliases spaced by an integer number of cycles per day from the preferred orbital frequency. The 1 cycle day^{-1} aliases, corresponding to periods of 0.1411 and 0.1953 days, cannot be ruled out unequivocally; however, it is noteworthy that the outburst data set also favors the 0.1640 day period. This agreement between two independent data sets strongly suggest that our preferred period is in fact the orbital period.

To determine the remaining orbital elements, we fit separately the quiescent and outburst data to sinusoids of the form

$$V(t, s) = \gamma(s) - K(s) \sin\left(\frac{2\pi[t - T_0(s)]}{P}\right),$$

where γ is the systemic velocity, K is the semiamplitude of the quiescent emission (or outburst absorption) lines, T_0 is the time of stellar conjunction, P (=0.1640 days) is the orbital period and s is the Gaussian separation.

If the line profiles were known to be symmetric around the orbit, the determination of the orbital elements would be straightforward. In general, however, the nonaxisymmetric nature of the disk emission often results in orbital-phase-dependent line profiles. Thus, solutions for orbital elements K, γ, and T_0 are not necessarily unique, but are usually functions of the Gaussian separation, s. Since the nature and extent of the asymmetry in the disk radiation is unknown, it is difficult to specify a value of s to use to measure the velocities. As a tool to explore the behavior of line asymmetries, we have found it useful to measure velocities based on a variety of separations, and then to plot the resulting orbital elements as a function of s, producing what we refer to as a "diagnostic diagram" (e.g., Shafter 1985; Shafter, Szkody, & Thorstensen 1986).

3.2. *The Quiescent Emission Lines*

We measured the quiescent emission lines using Gaussian separations ranging from 600 km s^{-1} to 1800 km s^{-1}. Again, all measurements were made using $\sigma = 300$ km s^{-1}. The diagnostic diagram for the quiescent Hα data is shown in Figure 3. The diagram shows the variation of the semiamplitude of the emission-line radial velocity curve, K, the fractional error in K, σ_K/K, the systemic velocity, γ, and the phase shift, $\Delta\phi$. The phase shift is defined as $\Delta\phi(s) = 2\pi[T_0(s) - T_0]/P$, where $T_0(s)$ is the time of conjunction determined using Gaussian separation, s, and T_0 is the true time of stellar conjunction. Since AR And is not an eclipsing system, the true time of stellar conjunction is not known reliably. Therefore, we have calculated a *relative* phase shift by defining $T_0 = T_0(s = 1200$ km s$^{-1})$. The quiescent diagnostic diagram is generally well behaved. The values of the γ-velocity and $\Delta\phi$ are nearly independent of s, suggesting that the emission from the accretion disk is reasonably axisymmetric.

The distribution of disk emission can be further explored by computing a Doppler map, or tomogram, which is an image displaying the line flux in velocity coordinates. A tomogram is constructed from line profiles obtained at a variety of orbital phases—the profile at a given phase providing a projection of the disk's velocity field onto the observer's line of sight. Since the accretion disk gas is in (near) Keplerian motion about the white dwarf with the inner disk material orbiting with the highest speed, a tomogram represents, in effect, an "inside-out" map of the disk emission. A complete description of the Doppler tomogram and its interpretation can be found in Marsh & Horne (1988).

Figure 4 shows a tomogram based on the Hα emission from our 39 quiescent-state spectra. The image is a simple Fourier-filtered back projection, as outlined in Horne (1992). The Fourier filtering, which sharpens up the point-spread function, helped to localize an enhanced emission region at low velocity (near $V_x \sim 0$ km s^{-1}, $V_y \sim 170$ km s^{-1}). With the exception of

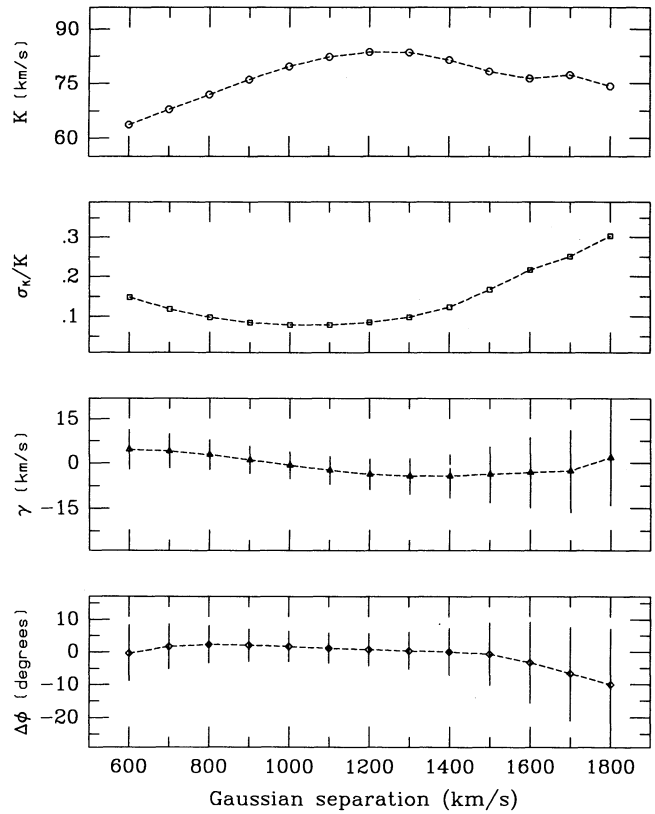

FIG. 3.—Diagnostic diagram for the quiescent Hα data. For values of the Gaussian separation greater than 1200 km s^{-1}, the K-velocity levels off at a value of ~ 85 km s^{-1}.

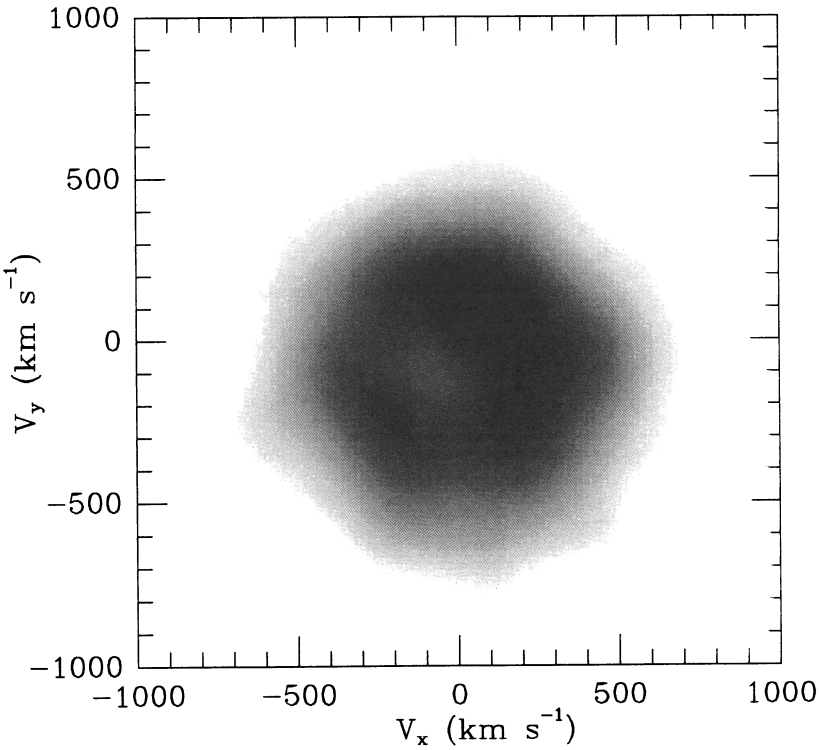

FIG. 4.—Doppler tomogram of the quiescent Hα data. The tomogram shows that the disk emission is relatively axisymmetric. The centroid of the emission is shifted downward by ~80 km s^{-1}—the approximate K-velocity of the white dwarf as estimated from these data. In addition, the tomogram clearly shows an enhanced emission region near the expected velocity coordinates of the secondary star.

this region, the tomogram displays a roughly symmetrical distribution of emission centered at ($V_x \sim 0$ km s^{-1}, $V_y \sim -80$ km s^{-1}). If the disk emission is nearly axisymmetric, the centroid of emission should be displaced downward (in the $-V_y$ coordinate) by an amount equal to the K-velocity of the white dwarf. Here, the Doppler map suggests that $K_{wd} \sim 80$ km s^{-1}, in good agreement with the value obtained from the diagnostic diagram.

The velocity coordinates of the excess emission region identified in Figure 4 suggest that it may be the result of emission from the vicinity of the secondary star. Normally, we would expect emission from the secondary star to be centered near ($V_x = 0$, $V_y = K_2$). However, since the radial velocity amplitude of the secondary star in AR And has not yet been measured, we cannot confirm this possibility. The small clockwise rotation of this emission region may be the result of a small phase shift in our radial velocity solution. Unfortunately, as AR And does not eclipse, we have no independent determination of the time of conjunction. The symmetry of the tomogram at velocities greater than ~400 km s^{-1} reveals that the (disk) emission is distributed uniformly with respect to the white dwarf. Bright spot emission, if it exists, does not contribute significantly to the overall Hα emission.

The variation of the K-velocity with Gaussian separation is consistent with this interpretation. The value of $K(s)$ increases slowly with increasing Gaussian separation until it levels off for values of $s > 1200$ km s^{-1}. This behavior is what one would expect if the low-velocity emission identified previously with the secondary star (which would be confined to low velocity and be 180° out of phase with the white dwarf) is spuriously lowering the measured value of K_{em}. If the excess emission is confined to the secondary star, and if we measure sufficiently far out into the line wings, the available evidence suggests that we can be reasonably confident that the measured value of K will provide a good measure of the white dwarf's orbital motion. The value of σ_K/K does not begin to rise significantly until s is increased beyond 1200 km s^{-1}, which is the point where the K-velocity has stabilized at a mean value of ~83 km s^{-1}.

We adopt the K-velocity determined at a separation of 1200 km s^{-1} ($K_{em} = 83 \pm 7$ km s^{-1}) as the quiescent emission-line amplitude. The quoted uncertainty is a formal error of the fit to a sinusoid and does not include possible sources of systematic

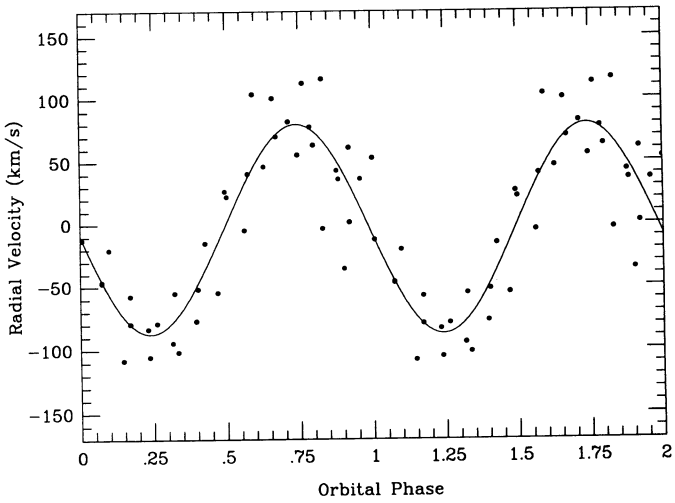

FIG. 5.—Radial velocity curve for the quiescent state Hα emission lines. The K-velocity is 83 ± 7 km s^{-1}.

TABLE 2

Hα Emission-Line Radial Velocities
($s = 1200$ km s^{-1})

HJD (2,440,000+)	Phase	Velocity (km s^{-1})
6,434.597.....	0.808	63.5
6,434.611.....	0.894	36.2
6,434.623.....	0.967	36.3
6,434.642.....	0.083	−46.8
6,434.654.....	0.156	−108.1
6,434.668.....	0.241	−83.4
6,434.682.....	0.327	−94.3
6,434.696.....	0.412	−51.9
6,434.707.....	0.479	−54.7
6,434.722.....	0.571	−4.6
6,434.733.....	0.638	46.5
6,434.747.....	0.723	82.2
6,434.759.....	0.796	77.8
6,434.774.....	0.888	42.9
6,435.601.....	0.930	1.7
6,435.615.....	0.016	−12.4
6,435.626.....	0.083	−46.2
6,435.642.....	0.180	−79.3
6,435.653.....	0.247	−105.4
6,435.667.....	0.333	−55.2
6,435.679.....	0.406	−77.2
6,435.695.....	0.504	26.6
6,435.708.....	0.583	40.6
6,435.724.....	0.680	70.3
6,435.736.....	0.754	55.8
6,435.750.....	0.839	−3.4
6,435.762.....	0.912	−35.7
6,436.626.....	0.180	−57.4
6,436.641.....	0.272	−78.9
6,436.653.....	0.345	−101.6
6,436.668.....	0.436	−15.1
6,436.680.....	0.510	22.1
6,436.695.....	0.601	103.8
6,436.706.....	0.668	100.6
6,436.723.....	0.772	112.4
6,436.734.....	0.839	115.8
6,436.749.....	0.930	61.4
6,436.762.....	0.010	53.2
6,436.778.....	0.107	−20.2

error (such as that introduced by the choice of the optimum Gaussian separation). The resulting radial velocities, given in Table 2, are folded with the orbital period and plotted as a function of orbital phase in Figure 5. Finally, to help identify possible variations in the emission-line profiles as a function of orbital phase, we have co-added the 39 individual quiescent spectra into 10 phase bins and plotted the resulting spectra in Figure 6. In agreement with the tomogram analysis, there is no obvious evidence for significant S-wave emission in the phased spectra of AR And.

3.3. *The Outward Absorption Lines*

During eruption, the spectrum of AR And develops broad and deep Balmer absorption lines characteristic of erupting dwarf novae. The mean spectra of AR And on the nights of 1991 December 10–12 are shown in Figure 7. The absorption-line strength clearly varies as AR And fades from maximum light. The variation is caused by a combination of the fading continuum level and the gradual filling in of the absorption by the strengthening emission cores. By the night of December 12 the absorption lines had become too weak for meaningful velocity measurements to be made. Thus, our absorption-line radial velocity measurements are based on the nights of

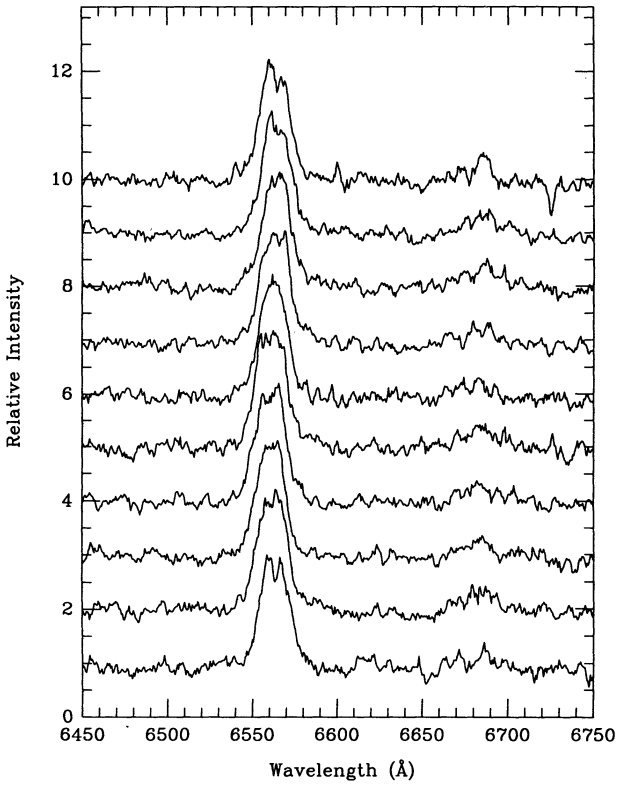

Fig. 6.—Quiescent Hα data binned into 10 phased spectra. Orbital phase increases from bottom to top in increments of 0.1, starting with phase 0.0. There is no obvious evidence for an *S*-wave in these data.

December 10 and 11 only. Because the line strengths and widths are variable, we have analyzed the two nights and the two absorption lines separately.

For all absorption-line velocity measurements, we again used Gaussian widths characterized by $\sigma = 300$ km s^{-1}. We have extended the Gaussian separation well beyond the maximum value used in the emission-line analysis because the absorption-line wings extend to significantly higher velocities than do the wings of the quiescent emission lines. This difference can be understood if a contribution to the Balmer absorp-

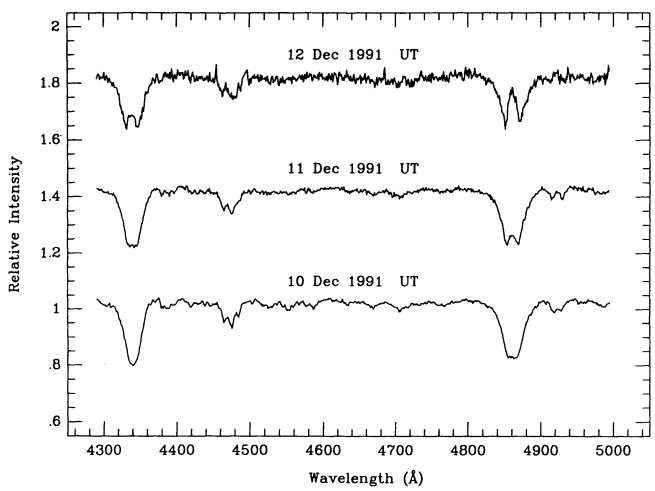

Fig. 7.—Mean outburst spectra

tion arises in the inner regions of the accretion disk (near the boundary layer with the white dwarf where the Keplerian velocities are high), while in quiescence the Balmer emission originates further out in the disk. In addition, it is possible that the higher density present in the inner regions of the outbursting disk may cause significant pressure broadening of the absorption lines in addition to the usual rotational Doppler broadening. Pressure broadening has been suggested to explain the broad absorption-line profiles seen in the UX UMa nova-like variable V3885 Sgr (Warner 1976; Herter et al. 1979). The absorption lines may therefore afford us the opportunity to probe further into the inner region of the accretion disk.

The diagnostic diagrams for the Hβ and Hγ data from the first night are shown in Figures 8 and 9. In the case of Hβ the K-velocity is relatively constant out to a value of $s \simeq 2000$ km s^{-1}. For separations beyond 2200 km s^{-1} the K-velocity slowly increases but so does the value of σ_K/K, indicating that the bandpasses are reaching the limits of the line wings. Since we would like to measure as far into the line wings as possible, we adopt $s = 2200$ km s^{-1} as the optimum separation. For this separation, the orbital solution yields a semiamplitude of 74 ± 10 km s^{-1}—slightly smaller, but consistent with the quiescent value. It is noteworthy that the K-velocity is not sensitive to the Gaussian separation. The average K-velocity for separations between 1000 and 2200 km s^{-1} is 75 km s^{-1}, in good agreement with the adopted value.

The diagnostic diagram for the Hγ data is similar to that for Hβ. The Gaussian separation can be increased to nearly 3000 km s^{-1} before the measurements become affected by noise in the continuum. For a separation of 2500 km s^{-1}, the K-velocity is 74 ± 10 km s^{-1} in agreement with the Hβ value. Once again the result is robust. The K-velocity varies by less than 5 km s^{-1} for Gaussian separations of 2000–3000 km s^{-1}. As was the case for the quiescent emission-line analysis, we have computed relative phase shifts. In this case, the phase shifts have been computed relative to the time of conjunction defined by $s = 2200$ km s^{-1} and $s = 2500$ km s^{-1} for Hβ and Hγ, respectively.

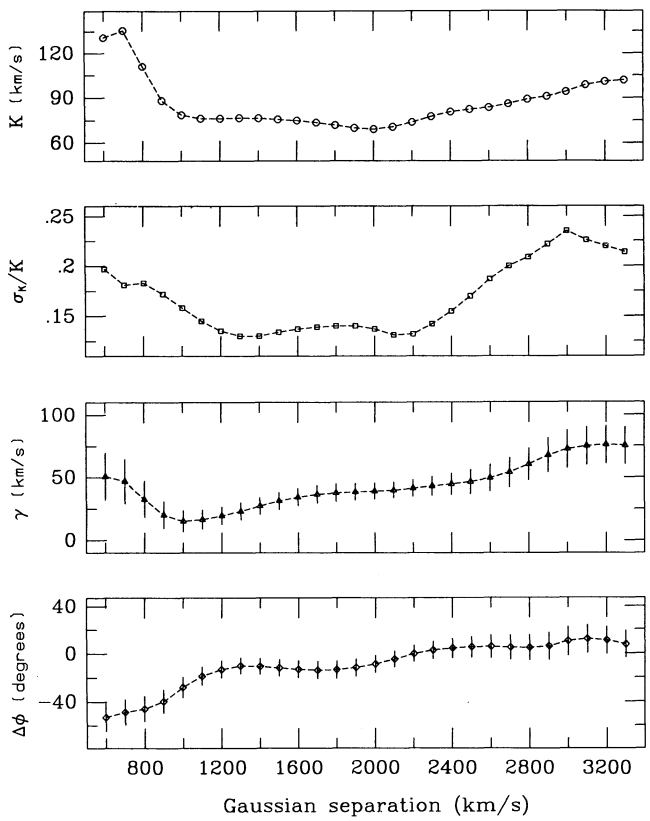

FIG. 8.—Diagnostic diagram for the December 10 outburst Hβ data. For small Gaussian separations, the orbital elements are biased because of emission in the line cores. At separations greater than 1200 km s^{-1}, the K-velocity levels off at a value of ~ 74 km s^{-1} until the separation exceeds the line width at the continuum ($s > 2200$ km s^{-1}).

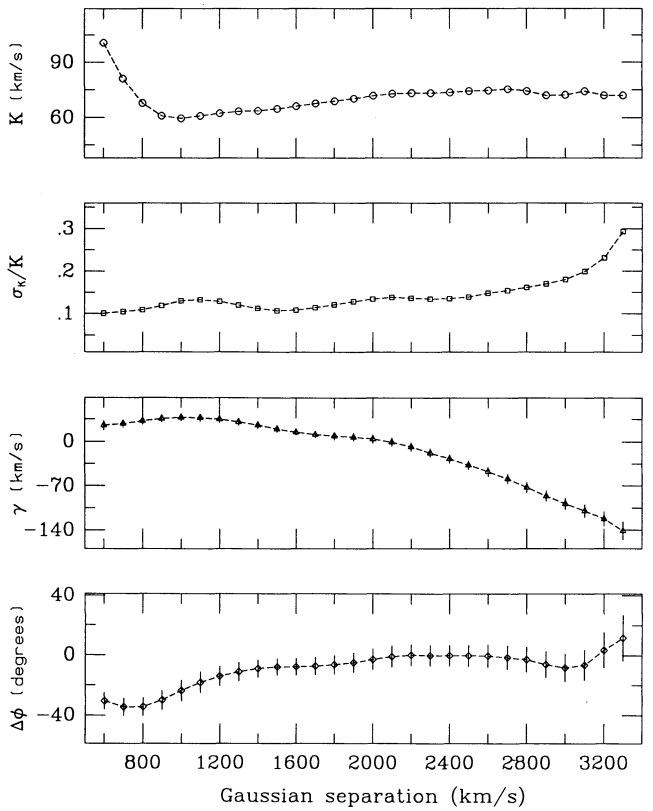

FIG. 9.—Diagnostic diagram for the December 10 outburst Hγ data. As for the Hβ data, the K-velocity levels off at a value of ~ 74 km s^{-1} for Gaussian separations greater than ~ 2000 km s^{-1}.

Despite the similarity between the Hβ and Hγ velocity amplitudes, the γ-velocities differ significantly. For double-Gaussian measurements, the γ-velocity is very sensitive to the slope of the nearby continuum. We have tried to minimize this effect by dividing each spectrum by a low-order polynomial fit to the continuum. All fits were made using the same polynomial order and continuum points to avoid introducing orbital-phase-dependent velocity shifts. The final γ-velocity is also sensitive to the presence of *non*–orbital-phase-dependent asymmetries in the line profiles, such as might be caused by blending of the line wing with a weak spectral feature. While the precise cause of the disparate γ-velocities is of some interest, it is unlikely to affect the derived velocity amplitudes, Indeed, it would be quite remarkable if the γ-velocity shift conspired to bring otherwise disparate Hγ and Hβ velocity amplitudes into close agreement.

Radial velocities based on measurements using our optimum Gaussian separations are given in Tables 3 and 4, and are plotted as a function of orbital phase in Figure 10. As

TABLE 3

ABSORPTION-LINE RADIAL VELOCITIES[a]

	Hγ		Hβ	
HJD (2,440,000+)	Phase	Velocity (km s^{-1})	Phase	Velocity (km s^{-1})
8,600.574.....	0.432	−33.2	0.444	21.6
8,600.585.....	0.504	−33.3	0.516	38.3
8,600.594.....	0.553	−4.6	0.564	45.1
8,600.604.....	0.619	7.2	0.630	29.9
8,600.612.....	0.667	81.4	0.678	86.6
8,600.623.....	0.733	53.1	0.745	84.7
8,600.631.....	0.780	53.8	0.792	169.8
8,600.642.....	0.849	−0.9	0.860	106.6
8,600.650.....	0.896	13.9	0.908	71.6
8,600.660.....	0.961	−20.6	0.973	28.9
8,600.668.....	0.009	−26.0	0.020	34.6
8,600.679.....	0.075	−52.0	0.087	32.8
8,600.687.....	0.124	−78.9	0.136	−25.6
8,600.698.....	0.189	−108.5	0.200	−69.6
8,600.706.....	0.237	−62.3	0.248	−4.2
8,600.717.....	0.303	−67.3	0.315	−72.9
8,600.725.....	0.352	−89.1	0.363	−24.4
8,600.735.....	0.416	−173.9	0.428	98.7
8,600.743.....	0.466	−89.5	0.478	54.5
8,600.755.....	0.535	−60.3	0.547	89.8
8,600.762.....	0.583	5.8	0.594	63.4
8,600.773.....	0.648	14.8	0.659	92.2
8,600.781.....	0.695	44.3	0.706	161.2
8,600.792.....	0.763	91.5	0.775	100.7
8,600.800.....	0.811	0.2	0.823	113.6
8,600.811.....	0.877	−13.7	0.889	88.3
8,600.818.....	0.924	−54.4	0.936	91.3
8,600.829.....	0.992	−13.4	0.003	67.7
8,600.837.....	0.040	−115.3	0.052	−16.8

[a] Gaussian separations of 2500 km s^{-1} (Hγ) and 2200 km s^{-1} (Hβ).

with the quiescent data, we have co-added the individual outburst spectra into 10 orbital phase bins. The phased spectra, plotted in Figure 11, show no obvious profile variations around the orbit.

As a further test of the disk symmetry, we computed Fourier-filtered Doppler tomograms for the outburst data. The

TABLE 4

ABSORPTION-LINE RADIAL VELOCITIES[a]

	Hγ		Hβ	
HJD (2,440,000+)	Phase	Velocity (km s^{-1})	Phase	Velocity (km s^{-1})
8,601.572.....	0.518	41.8	0.529	45.4
8,601.583.....	0.587	25.3	0.599	57.7
8,601.591.....	0.635	67.4	0.646	101.9
8,601.602.....	0.700	115.9	0.712	77.3
8,601.610.....	0.750	91.2	0.761	87.5
8,601.621.....	0.818	63.5	0.829	50.0
8,601.629.....	0.865	38.0	0.877	76.0
8,601.640.....	0.933	14.1	0.945	68.3
8,601.648.....	0.981	10.1	0.992	14.2
8,601.658.....	0.044	11.8	0.056	−10.9
8,601.666.....	0.092	25.4	0.103	−15.4
8,601.677.....	0.157	−23.8	0.169	−34.7
8,601.685.....	0.206	−43.1	0.217	−23.6
8,601.695.....	0.272	11.2	0.284	−137.2
8,601.703.....	0.320	−12.9	0.332	−129.1

[a] Gaussian separations of 2100 km s^{-1} (Hγ) and 1800 km s^{-1} (Hβ).

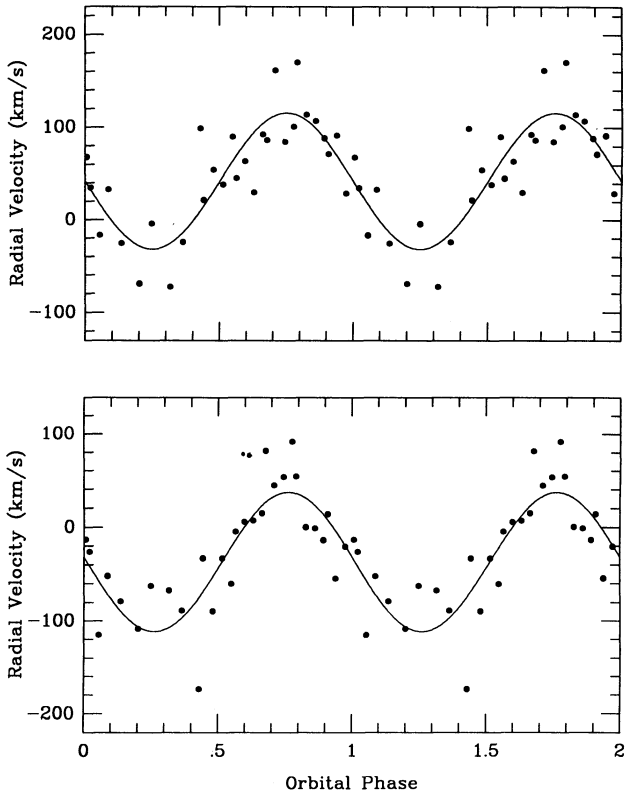

FIG. 10.—Radial velocity curves for the outburst state Hβ (*top*) and Hγ (*bottom*) absorption lines. In both cases the *K*-velocity is 74 ± 10 km s^{-1}.

calculations were done by inverting the spectra and treating the Hβ and Hγ absorption lines as though they were emission lines. The resulting tomograms, shown in Figure 12, indicate regions of the disk's surface that have the deepest absorption, rather than the strongest emission as in a standard tomogram. The tomogram for Hβ (Fig. 12*a*) shows a nearly symmetrical ring, which is offset downward by ~75 km s^{-1} (the *K*-velocity of the white dwarf as determined from these data). The tomogram for Hγ (Fig. 12*b*) is also offset by ~75 km s^{-1}, but is centrally peaked. The difference is a consequence of the emission-line core in the Hβ profile, which can be seen in the summed data shown in Figure 7. Absorption lines with emission cores effectively mimic double-peaked emission lines when computing the tomogram. On the other hand, the deep and symmetric Hγ absorption line is analogous with a single-peaked emission feature. Despite their differences at low velocity, the tomograms appear axisymmetric at high velocities, suggesting that the absorption-line wings are relatively free of orbital-phase-dependent distortions.

On the following night, significant changes occur, as can be seen from the diagnostic diagrams in Figures 13 and 14. One notable difference is that the emission cores are becoming more prominent, particularly in the case of Hβ. This difference is a result of the emission-line Balmer decrement being steeper than the absorption-line decrement. The contamination of the velocity measurements by the emission-line cores for separations $\lesssim$1000 km s^{-1} is clearly evident in the diagnostic diagram for the Hβ line. The value of σ_K/K begins to increase for separations beyond ~1800 km s^{-1}. At this separation, the *K*-velocity is 89 ± 13 km s^{-1}. Again, the value is not terribly sensitive to the value of *s*. For values of $s > 1800$ km s^{-1}, the

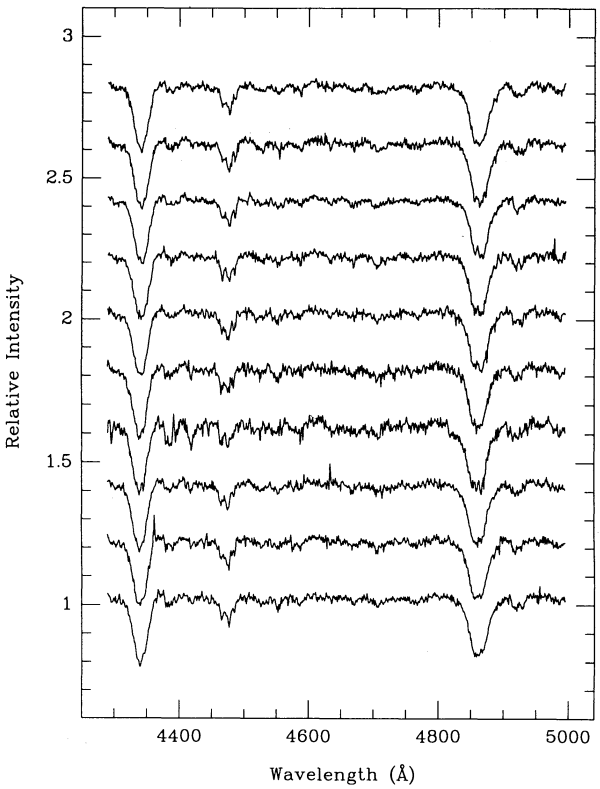

FIG. 11.—Outburst data binned into 10 phased spectra. Orbital phase increases from bottom to top in increments of 0.1, starting with phase 0.0. There is no obvious evidence for orbital-phase-dependent line profile variations in these data.

K-velocity has leveled off to a mean value of ~ 83 km s^{-1}, not inconsistent with the previous night and in good agreement with the quiescent K-velocity.

The behavior of Hγ on the second night is quite different from that of Hβ. Since there is no sharp increase in the value of σ_K/K, it is not obvious what value of the Gaussian separation to use when determining the K-velocity. It is clear, however, that regardless of the choice, of s, the value of K will be significantly lower than that obtained from measurements of Hβ. Fortunately, the value of K does not vary significantly for value of $s > 1000$ km s^{-1} (i.e., separations that exclude the emission core). For Hγ on the second night we adopt the mean of the K-velocities corresponding to values of s between 1200 and 3200 km s^{-1}, finding $K_{abs} = 55 \pm 9$ km s^{-1}. Because the orbital period is known precisely enough to easily bridge the two nights of observation, we have used the fiducial times, $T_0(s = 2200$ km s$^{-1})$ and $T_0(s = 2500$ km s$^{-1})$, for Hβ and Hγ determined on the previous night to explore the variation of the time of conjunction as a function of Gaussian separation ($\Delta\phi(s)$).

A summary of the orbital solutions for the quiescent and outburst data is given in Table 5. Taking a mean of the absorption-line amplitudes for Hβ and Hγ on both nights we find $\langle K_{abs} \rangle = 73 \pm 14$ km s^{-1}. If, as the best estimate of the white dwarf's amplitude, we adopt the mean of the emission- and absorption-line amplitudes (weighted equally), we find $K_{wd} \simeq 80$ km s^{-1}. It is worth remarking, however, that three of the four absorption-line amplitudes are lower than the quiescent K-velocity. In essentially all cases where the K-velocity of the white dwarf has been *predicted* independently, based on photometric orbital solutions (e.g., see Shafter 1992, and references therein), the predicted K-velocity is in fact *lower* than the measured value. In this context, it is tempting to explain the small discrepancy between our emission- and absorption-line amplitudes as being the result of a slightly biased emission-line amplitude. If so, it may be that the best estimate of the K-velocity of the white dwarf in AR And and is given by the absorption-line amplitude alone. In this case we return to the slightly lower value, $K_{wd} = 73 \pm 14$ km s^{-1}.

4. DISCUSSION

The radial velocity studies of AR And in quiescence and in eruption yield consistent results. The similarity between the quiescent and outburst solutions is noteworthy in part because the quiescent data were obtained using a different telescope, spectrograph, and detector and were based on measurements of Hα rather than the Hβ and Hγ lines used in the outburst observations. The agreement between the quiescent and outburst data is robust in the sense that the derived amplitudes appear to be quite insensitive to the position in the line profile where the velocity measurements were made. It is also encouraging that the absorption-line amplitudes found by Szkody et al. (1990) ($K_{H\gamma} = 88 \pm 7$ km s^{-1}, $K_{H\beta} = 79 \pm 22$ km s^{-1}) are in good agreement with our quiescent and outburst solutions.

The similarity of the quiescent and outburst radial velocity amplitudes does not insure that the derived K-velocity is free from bias. However, the agreement does require that, if bias is present, it must be affecting the quiescent emission lines and the outburst absorption lines in a similar fashion. Such conspiratorial behavior would be quite remarkable given that the emission and absorption lines are formed under radically different physical conditions. To further explore the disk structure, we computed Doppler tomograms based on the quiescent emission-line and outburst absorption-line data. The emission-line tomogram indicates that the Hα emission arises primarily in the accretion disk during quiescence and that bright spot emission is not significant. The tomograms computed from the

TABLE 5

ORBITAL ELEMENTS[a]

A. QUIESCENT Hα

Parameter	Value
Time of conjunction, T_0 (HJD)	2,446,434.628 ± 0.004
Systemic velocity, γ (km s^{-1})	−4 ± 5
Semiamplitude, K_{em} (km s^{-1})	83 ± 7

B. OUTBURST Hγ AND Hβ

Parameter	Hγ	Hβ
Dec 10		
Time of conjunction, T_0 (HJD)	2,448,600.011	2,448,600.009
Systemic velocity, γ (km s^{-1})	−38 ± 7	42 ± 7
Semiamplitude, K_{abs} (km s^{-1})	74 ± 10	74 ± 10
Dec 11		
Time of conjunction, T_0 (HJD)	2,448,601.011	2,448,601.009
Systemic velocity, γ (km s^{-1})	28 ± 6	8 ± 9
Semiamplitude, K_{abs} (km s^{-1})	55 ± 9	89 ± 13

[a] $P = 0.1640$ days; $e = 0$ (assumed).

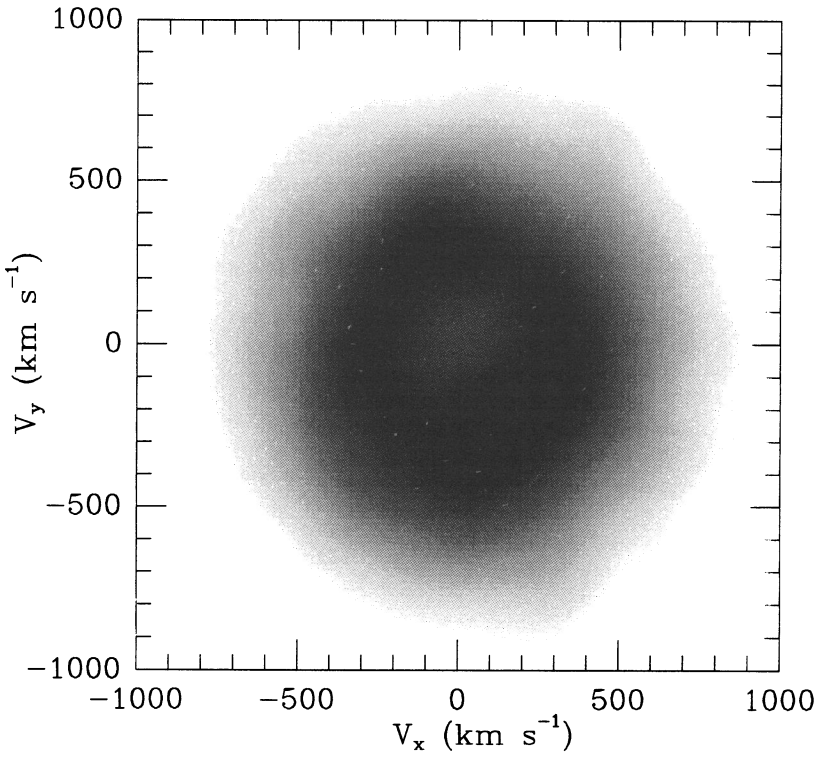

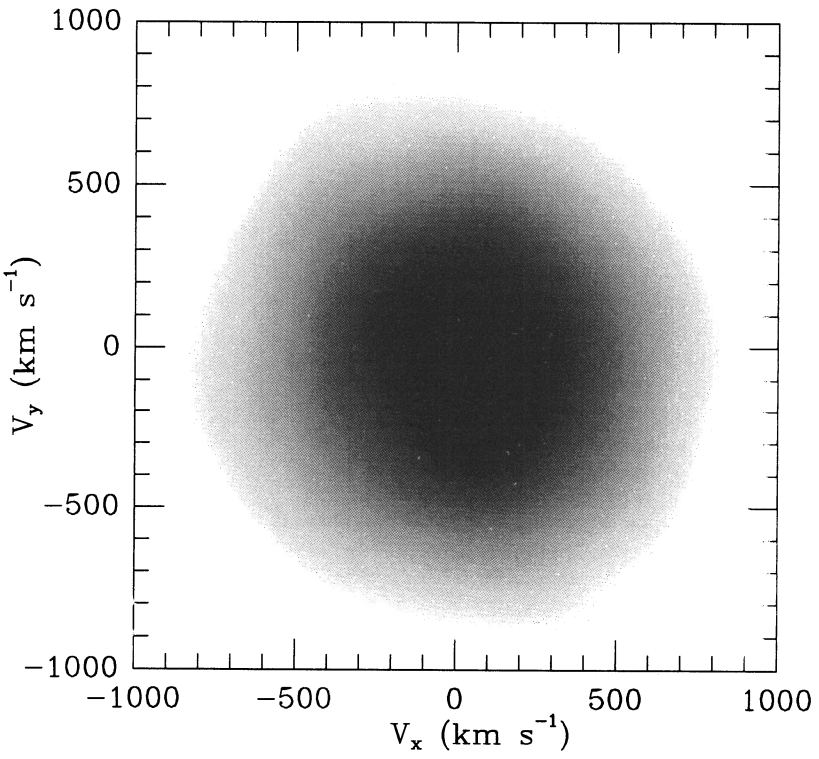

FIG. 12*b*

FIG. 12.—Doppler tomograms for the outburst data: (*a*) Hβ and (*b*) Hγ. The tomograms, which were computed by inverting the absorption-line profiles, reveal that the disk absorption, like the Hα emission, appears relatively axisymmetric. In both cases, the centroid of the absorption is shifted downward by ~75 km s^{-1}—the approximate *K*-velocity of the white dwarf as estimated from these data. The central depression seen in the Hβ tomogram results from the emission-line cores in the absorption profiles.

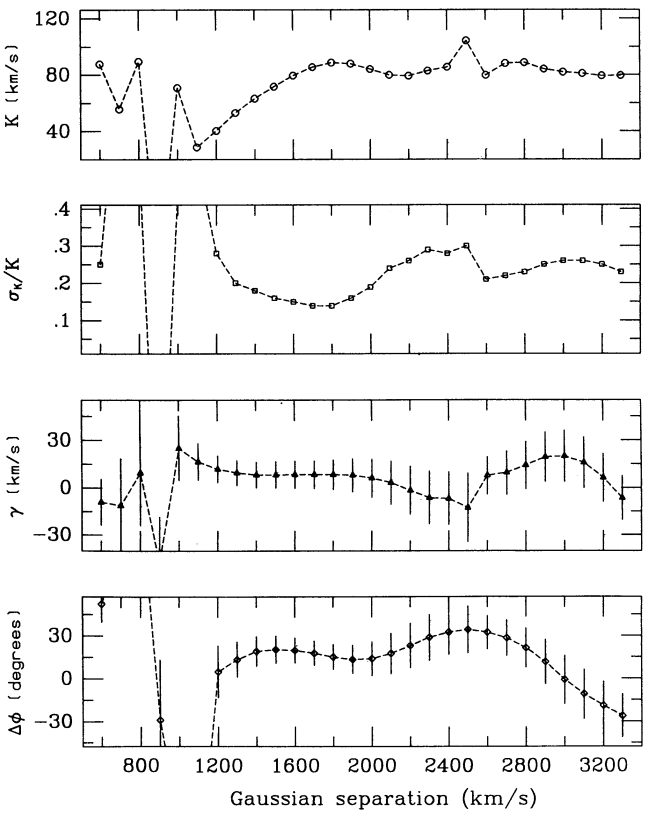

FIG. 13.—Diagnostic diagram for the December outburst Hβ data. Same as Fig. 5, except that the emission core is much stronger, resulting in spurious measurements at small Gaussian separations. The K-velocity at the point where the measurement error rises steeply ($s = 1800$ km s^{-1}) is 89 km s^{-1}.

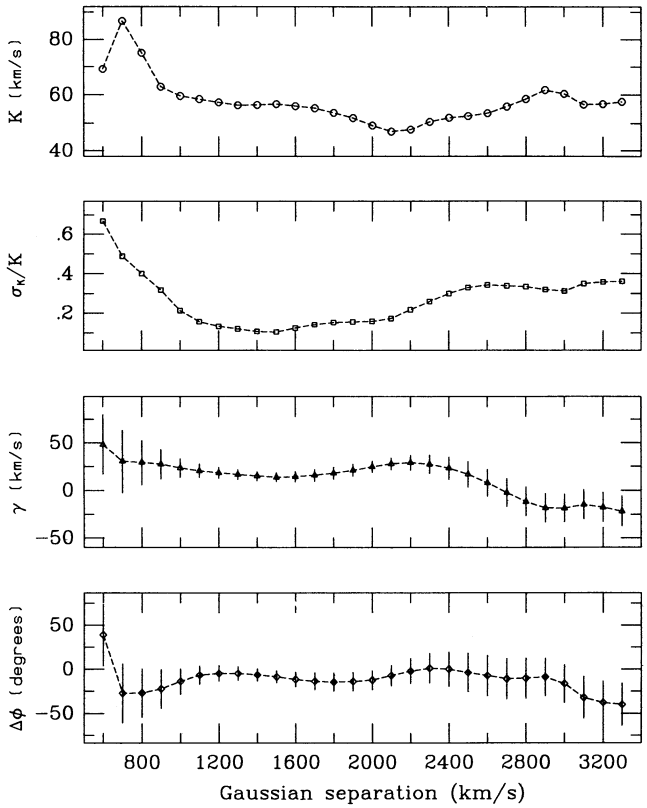

FIG. 14.—Diagnostic diagram for the December 11 outburst Hγ data. The best K-velocity is difficult to determine from these data. Aside from the dip occurring at $s \simeq 2100$ km s^{-1}, the K-velocity remains relatively constant near a mean value of 55 km s^{-1}.

absorption-line spectra are also consistent with an axisymmetric disk structure during outburst. In summary, the available evidence suggest that the disk emission (and absorption) lines do trace the motion of the white dwarf in AR And.

Despite the encouraging results for AR And, there is ample evidence that this system is the exception rather than the rule. The radial velocity curves in many cataclysmic variable systems are known to be severely biased. The principal evidence comes from studies of eclipsing systems, or double-lined systems, or both, that reveal significant phase lags between spectroscopic and photometric conjunction. Subsequent Doppler tomographic studies of many of these systems show that the emission originates primarily in a localized region of the accretion disk near the point where the interstar mass transfer stream impacts the disk. In a recent study, Shafter (1992) has shown that the phase lags are a function of both eruptive behavior and orbital period. The largest phase lags are observed for nova-like variables with periods just above the period gap, the so-called SW Sex stars (Thorstensen et al. 1991), while the smallest phase lags are found in dwarf novae with periods above the gap.

Doppler tomograms of the SW Sex stars reveal that the emission in these systems comes primarily from the general vicinity of the bright spot, with line emission from the disk being significantly weaker (Kaitchuck 1994). It is not surprising that the radial velocity curves of such systems do not accurately reflect the orbital motion of the white dwarfs. The single-peaked emission lines typical of the SW Sex stars (and nova-like variables in general) is consistent with emission from a localized region as opposed to the full disk face. On the other hand, Doppler tomograms and emission-line profiles of dwarf novae suggest that dwarf novae have a substantial emission component from the entire disk. In addition to the principal disk emission component, there is often a component from the bright spot region that gives rise to the so-called S-wave observed in trailed spectrograms. Dwarf nova systems where the S-wave emission is either absent or is clearly delineated from the overall disk emission offer the best opportunity to measure a meaningful K-velocity for the white dwarf.

The empirical evidence compiled by Shafter (1992) suggests that the phase lags are smallest in dwarf novae above the period gap. A likely explanation is that, in dwarf novae below the gap, the SU UMa systems, the mass ratios are believed to be relatively extreme (e.g., see Whitehurst 1988). In these extreme mass ratio systems the bright spot is expected to be farther from the line of centers than in systems with mass ratios near unity. Since any excess emission associated with the bright spot will be out of phase with the white dwarf's orbital motion, the further the bright spot is from the line of centers, the greater the phase difference. Thus, dwarf novae below the gap are more likely to exhibit phase lags than are their longer period counterparts. As noted previously, Hessman's (1986) study of the long-period dwarf nova SS Cyg, provides a good example. Although SS Cyg is not eclipsing, the phase lag was determined to be insignificant from a comparison of the emission-line orbit with that of the secondary star determined at quiescence. Not surprisingly, Hessman (1986) found good agreement between the amplitudes of the emission- and

absorption-line radial velocity curves. Given that AR And is a dwarf nova above the period gap, perhaps it is not surprising that the emission- and absorption-line radial velocity amplitudes are roughly consistent. Unfortunately, the phase relationship between the secondary star, disk emission, and disk absorption are unknown at present. It would be useful to know the relative phase between our quiescent and outburst data, but such a comparison will not be possible until the orbital period is known with greater precision.

A more crucial test of our AR And result would be provided by a measurement of the secondary star's radial velocity curve. If the disk emission lines do indeed reflect the white dwarf's orbital motion, then the quiescent absorption lines originating in the secondary star should be precisely 180° out of phase with the emission lines. The presence of a significant phase offset between the emission- and absorption-line radial velocity curves would cast doubt on the reliability of our determination of K_{wd}. In the event that the phase difference is 180°, as expected, an estimate of the masses in AR And may be possible. If the secondary star was determined to be near the main sequence, a knowledge of its radial velocity amplitude would enable a direct determination of the component masses (e.g., Robinson 1976). Since reliable masses for cataclysmic variables are so rare, clearly AR And is an object worthy of further study.

We wish to acknowledge the use of data obtained from the AAVSO international database operated at AAVSO Headquarters, 25 Birch Street, Cambridge, MA 02138. We thank Janet Mattei and the AAVSO observers for their efforts in monitoring dwarf novae. We thank Tod Ramseyer for assistance in acquiring the McDonald data. This work has been supported in part by NSF grant AST-91-15131 (A. W. S.).

REFERENCES

Feinswog, L., Szkody, P., & Garnavich, P. 1988, AJ, 96, 1702
Feldt, A. N., & Chincarini, G. 1988, PASP, 92, 528
Herter, T., Lacasse, M. G., Wesemael, F., & Winget, D. E. 1979, ApJS, 39, 513
Hessman, F. V. 1986, ApJ, 300, 794
Horne, K. 1992, in Proc. San Diego Workshop on Fundamental Properties of Cataclysmic Variables, ed. A. W. Shafter (San Diego: [Available from A. W. Shafter]), 23
Kaitchuck, R.H. 1994, in ASP Conf. Ser., 56, Interacting Binary Stars, ed. A. W. Shafter (San Francisco: ASP), 287
Kaitchuck, R. H., Mansperger, C. S., & Hantzios, P. A. 1988, ApJ, 330, 305
Lomb, N. R. 1972, Ap&SS, 39, 447
Marsh, T. R., & Horne, K. 1988, MNRAS, 235, 269
Mattei, J. A. 1993, private communication (observations from the AAVSO international database)
Patterson, J. 1979, ApJ, 234, 978
Press, W. H., & Rybicki, G. B. 1989, ApJ, 338, 227
Robinson, E. L. 1976, ApJ, 203, 485
Robinson, E. L., Shafter, A. W., & Balachandran, S. 1991, ApJ, 374, 298
Robinson, L. B., & Wampler, E. J. 1972, PASP, 84, 161
Scargle, J. D. 1982, ApJ, 263, 835
Schneider, D. P., & Young, P. 1980, ApJ, 238, 946
Shafter, A. W. 1983, ApJ, 267, 222
———. 1985, in Cataclysmic Variables and Low Mass X-Ray Binaries, ed. D. Q. Lamb & J. Patterson (Dordrecht: Reidel), 355
———. 1992, in Proc. San Diego Workshop on Fundamental Properties of Cataclysmic Variables, ed. A. W. Shafter (San Diego: [Available from A. W. Shafter]), 39
Shafter, A. W., Hessman, F. V., & Zhang, E. H. 1988, ApJ, 327, 248
Shafter, A. W., Szkody, P., & Thorstensen, J. R. 1986, ApJ, 308, 765
Szkody, P., Piché, F., & Feinswog, L. 1990, ApJS, 73, 441
Thorstensen, J. R., Ringwald, F. A., Wade, R. A., Schmidt, G. D., & Norsworthy, J. E. 1991, AJ, 102, 272
———. 1992, in Proc. San Diego Workshop on Fundamental Properties of Cataclysmic Variables, ed. A. W. Shafter (San Diego: [Available from A. W. Shafter]), 61
Warner, B. 1976, in IAU Symp. 73, The Structure and Evolution of Close Binaries, ed. P. Eggleton, S. Mitton, & J. Whelan (Dordrecht: Reidel), 85
Welsh, W., Horne, K., & Gomer, R. 1993, ApJ, 410, L39
Whitehurst, R. 1988, MNRAS, 232, 35